Inorganic Chemistry
Cite This: Inorg. Chem. 2020, 59, 717−729
Article
pubs.acs.org/IC

High-Pressure Crystallographic and Magnetic Studies of Pseudo-D_{5h} Symmetric Dy(III) and Ho(III) Single-Molecule Magnets

Marie S. Norre,[†] Chen Gao,[†] Sourav Dey,[‡] Sandeep K. Gupta,[‡] Aditya Borah,[‡] Ramaswamy Murugavel,[‡] Gopalan Rajaraman,[‡] and Jacob Overgaard*[,†]

[†]Department of Chemistry, Aarhus University, Langelandsgade 140, 8000 Aarhus C, Denmark
[‡]Department of Chemistry, Indian Institute of Technology Bombay, Mumbai 400076, India

Supporting Information

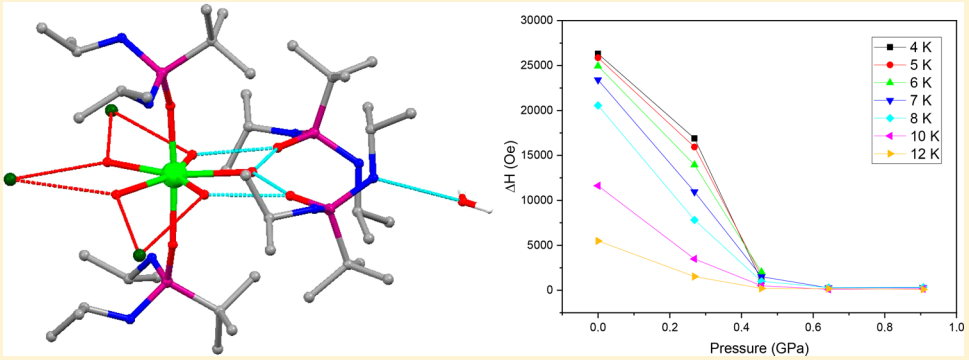

ABSTRACT: Single-ion magnets based on lanthanide ions in pseudo-D_{5h} symmetry have gained much attention in recent years as they are reported to possess a large blocking temperature and a large barrier for magnetization reversal. Magneto-structural correlations reveal that the axial O−Ln−O angle is an important parameter to control the barrier, and while it can be fine-tuned by chemical modification, an alternative would be to utilize hydrostatic pressure. Herein, we report the crystal structures and static magnetic properties of two air-stable isostructural lanthanide SIMs under applied pressures. The complexes exhibit pseudo-D_{5h} symmetry around the Ln(III)-ion (Ln = Dy or Ho), which coordinates to five equatorial water molecules and two large neutral phosphonic diamide ligands along the axial direction. High-pressure single-crystal X-ray diffraction experiments revealed two phase-transitions and an increasing deviation from D_{5h}-symmetry between ambient pressure and 3.6 GPa. High-pressure direct-current magnetic measurements of the Dy(III) compound showed large steps in the hysteresis loops near zero field, indicative of quantum tunneling of magnetization (QTM). These steps grow in size with increasing pressure, suggesting that QTM becomes progressively more active, which correlates well with the pressure-induced increased overall deviation from pseudo-D_{5h} symmetry and decreasing axial O−Dy−O angle. A strong temperature dependence of the step size is seen at 0.3 GPa, which shows that the SMM character persists even at this pressure. To understand the origin of significant variation in the tunneling probability upon pressure, we performed a range of *ab initio* calculations based on the CASSCF/RASSI-SO/SINGLE_ANISO method on both Dy and Ho complexes. From the energies and magnetic anisotropy of the m_J sublevels, we find a complex variation of the energy barrier with pressure, and using a constructed geometrical parameter, *R*, taking into account changes in both bond angles and distances, we link the magnetic properties to the first coordination sphere of the molecules.

INTRODUCTION

Single-molecule magnets (SMMs) are molecules which exhibit blocking of magnetization below a certain temperature, denoted by T_B. If the molecule has a bistable magnetization and a sufficiently high T_B, then it would be possible to use these molecules for high density data storage by magnetizing them to be either spin-up or -down, reaching a state which is maintained. For any technological implementation of SMMs to be a feasible, we first need to locate systems with T_B higher than the boiling point of liquid nitrogen (77 K).

The discovery of the first SMM, a mixed-valence Mn_{12} cluster, dates back to 1993.[1,2] For obvious reasons improved compounds were subsequently sought, especially among transition metal complexes often containing several metal ions.[3] Then, in 2003, Ishikawa discovered the first mononuclear lanthanide SMM $(TbPc_2)^-$ (Pc = dianion of phthalocyanine),[4] and this prompted a search for SMM properties among both lanthanide and transition-metal monometallic systems.[5] Eventually, this quest led to the discovery of a monometallic Dy(III) SMM having a blocking temperature of 60 K.[6,7] This reinforced the belief that

Received: October 7, 2019
Published: December 12, 2019

DOI: 10.1021/acs.inorgchem.9b02962
Inorg. Chem. 2020, 59, 717−729

mononuclear lanthanide complexes were ideal candidates for delivering SMMs with T_B above 77 K and already two years later another mononuclear Dy(III) SMM was discovered with T_B of 80 K.[8]

The energy barrier U_{eff} that hinders the equilibration of magnetization is a useful alternative to the above-mentioned T_B when it comes to measuring the quality of an SMM. This energy barrier, which can be extracted using dynamic ac susceptibility measurements,[9] is intimately connected to the magnetic anisotropy of the SMM, and one widespread guiding principle in synthetic research is to maximize the magnetic anisotropy. For lanthanide systems, one way to achieve this goal is to choose coordinating ligands that complement the anisotropic shape of the 4f electron density of the central metal ion,[10] which is generally described as either oblate (flattened sphere) or prolate (elongated sphere). Examples of oblate-density ions are Dy(III) and Ho(III), and it has been shown that special ligand fields where two ligands approach the lanthanide in a trans-configuration will strongly amplify the magnetic anisotropy of these ions and thus their SMM potential.[11] The perfectly linear two-coordinate lanthanide complex is, however, difficult to synthesize because it exposes the vacant equatorial coordination sites and such systems are highly reactive.[12] To alleviate these problems, it is possible either to apply loosely bonded equatorial ligands or to use very bulky axial ligands to impede the coordination in the equatorial plane.[13]

Much of the progress in SMM research has relied on the synthesis of classes of compounds with related structures and subsequently correlating their magnetic properties with variations of structural or electronic properties. However, this approach is often limited by the fact that the electronic properties, such as the ligand field strength or orbital populations, have to be calculated *ab initio* and are thus subject to unknown limitations which for lanthanides potentially quite severe. Similarly, it is not always possible to synthesize and crystallize complete compound classes observing isomorphous crystal structures. Inevitably, this leads to differences in crystal packing and intermolecular interactions having an unknown effect on the magnetic properties and preventing systematic studies. On the contrary, it is possible to study the structural and magnetic properties of the exact same magnetic molecule in a continuously changing range of environments by enclosing a single-crystal sample in a pressure cell and vary its structure by application of an external pressure. Studying SMMs under applied hydrostatic pressure can be used to investigate how changes in structure affect the SMM properties as well as to study the stability of these properties under geometrical changes to the magnetic molecule. The latter is of interest since previous studies have shown that structural changes of this nature may occur when SMMs are placed on a surface as would be necessary for their practical use.[14] To the best of our knowledge, the first combined high-pressure X-ray crystallography and magnetic measurements on SMMs was reported in 2005.[15] However, only a few studies using this method of investigation of SMMs have been reported since then,[16−20] and none of these have involved lanthanide ions.

In this contribution, we therefore present results of high-pressure structural and magnetic investigations of two Ln(III) compounds, denoted **1Dy** and **1Ho**, in addition to theoretical calculations of the electronic structure in the experimental high-pressure geometries. We have previously reported on the synthesis, ambient-pressure crystal structure, and magnetic properties of these compounds.[3,21] Importantly, these compounds are air- and moisture-stable, which is clearly a desired but rather uncommon property.[21] Their crystal structure consist of a central trivalent lanthanide ion in a pseudo-D_{5h} symmetry, which coordinates to two large neutral axial phosphonic diamide ligands and five equatorial water molecules (see Figure 1).

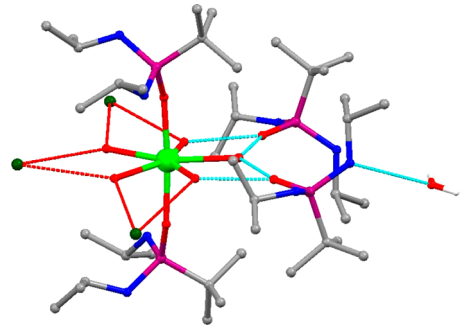

Figure 1. Structure of **1Ho**. Gray, C; red, O; light green, Ho; dark green, I; dark blue, N; purple, P. The hydrogens (white) have been omitted for clarity except on the lattice water. The thin dashed lines represent hydrogen bonds.

EXPERIMENTAL DETAILS

Synthesis. The synthesis of both **1Dy** and **1Ho** has previously been described by Murugavel et al.[3,21]

Ambient and High-Pressure Single-Crystal X-ray Crystallography. The structures of **1Ho** and **1Dy** were measured on a Rigaku Oxford Diffraction SuperNova using an Atlas CCD detector and a molybdenum X-ray source. The ambient-pressure structures of both compounds were measured on a crystal in Paratone-N on a nylon loop at 100 K. The pressure data was measured at ambient temperature on a crystal inside an Almax Plate Diamond Anvil Cell (DAC) with Daphne 7373 as the pressure-transmitting medium. A ruby was added to allow the determination of the pressure inside the DAC from the known pressure dependency of the fluorescence wavelength shift.

The structure of **1Dy** was measured at seven different pressures on the same crystal and two additional pressures (1.62 and 2.05 GPa) on a different crystal. The structure of **1Ho** was measured at six different pressures on a crystal from the same batch as the one used for ambient-pressure measurements, and the unit cell was measured at one additional pressure (1.26 GPa) on a crystal from a different batch.

Magnetic Measurements. The ambient-pressure magnetic data of **1Ho** was measured outside a pressure cell with a magnetic field sweep rate of 270 Oe/s.[3] The magnetic data at elevated pressures was measured in a Quantum Design HMD High Pressure Cell made of BeCu alloy on a Quantum Design Physical Property Measurement System (PPMS) equipped with a 9 T magnet using a vibrating sample magnetometer (VSM). The measurements were made on approximately 0.4 mg of crystalline powder sample with Daphne 7373 as the pressure-transmitting medium and a small piece of lead to be able to center the cell and to measure the pressure inside the cell. Background measurements were conducted using a fully assembled cell containing only the lead piece and Daphne 7373.

The Ho sample was measured at three different pressures, and this data was corrected for the background. The Dy sample was measured at ambient pressure (inside the pressure cell) and at four different pressures. In this case the background data was measured, but the intensity of these were insignificant compared to that of the data. However, below 7 K the signal from lead was removed from the data.

Computational Details. The hydrogen positions of **1Dy** and **1Ho** at all pressure points have been optimized using Gaussian09

DOI: 10.1021/acs.inorgchem.9b02962
Inorg. Chem. 2020, 59, 717−729

Table 1. Selected Crystallographic Details for 1Dy

pressure (GPa)	space group	a (Å)	b (Å)	c (Å)	β (deg)	V (Å^3)
0.53(2)	$I2/a$	25.082(2)	13.144(3)	22.0288(17)	113.889(9)	6639.6(19)
0.9(2)	$I2/a$	24.6651(13)	12.77(2)	22.117(10)	114.267(6)	6350.8(12)
1.32(3)	$I2/a$	22.0670(12)	12.455(3)	24.3378(16)	114.267(7)	6098.2(14)
1.62(3)	$P2_1/c$	22.6350(9)	12.6671(5)	22.147(2)	113.066(7)	5842.3(7)
2.05(3)	$P2_1/c$	22.4950(8)	12.5803(4)	22.0201(18)	112.957(6)	5738.0(6)
2.21(4)	$P2_1/c$	22.4635(12)	12.541(2)	21.9554(14)	112.970(7)	5694.6(12)
3.02(5)	$P2_1/c$	22.258(10)	12.371(2)	21.7548(12)	112.786(6)	5522.8(10)
3.26(5)	$P2_1/c$	22.211(10)	12.341(2)	21.7047(12)	112.7660(12)	5485.9(10)
3.59(6)	$P2_1/c$	22.1440(11)	12.306(2)	21.6283(13)	112.728(6)	5435.9(11)

Table 2. Selected Crystallographic Details for 1Ho

pressure (GPa)	space group	a (Å)	b (Å)	c (Å)	β (deg)	V (Å^3)
0.47(2)	$I2/a$	24.924(12)	13.0723(5)	22.107(3)	114.24(3)	6568(4)
0.51(2)	$I2/a$	24.795(12)	12.9712(5)	22.089(3)	114.25(4)	6478(4)
0.70(2)	$I2/a$	22.066(3)	12.7745(5)	24.527(11)	114.24(3)	6304(3)
1.26(3)	$P2_1/c$	22.002(9)	12.4447(12)	24.254(11)	114.11(6)	6061(4)
1.42(2)	$P2_1/c$	22.607(4)	12.6890(5)	22.125(5)	112.96(3)	5843.9(19)
3.07(5)	$P2_1/c$	22.061(4)	12.4423(6)	21.519(5)	112.03(3)	5475(2)
3.61(4)	$P2_1/c$	21.885(7)	12.4064(8)	21.315(7)	111.50(4)	5384(3)

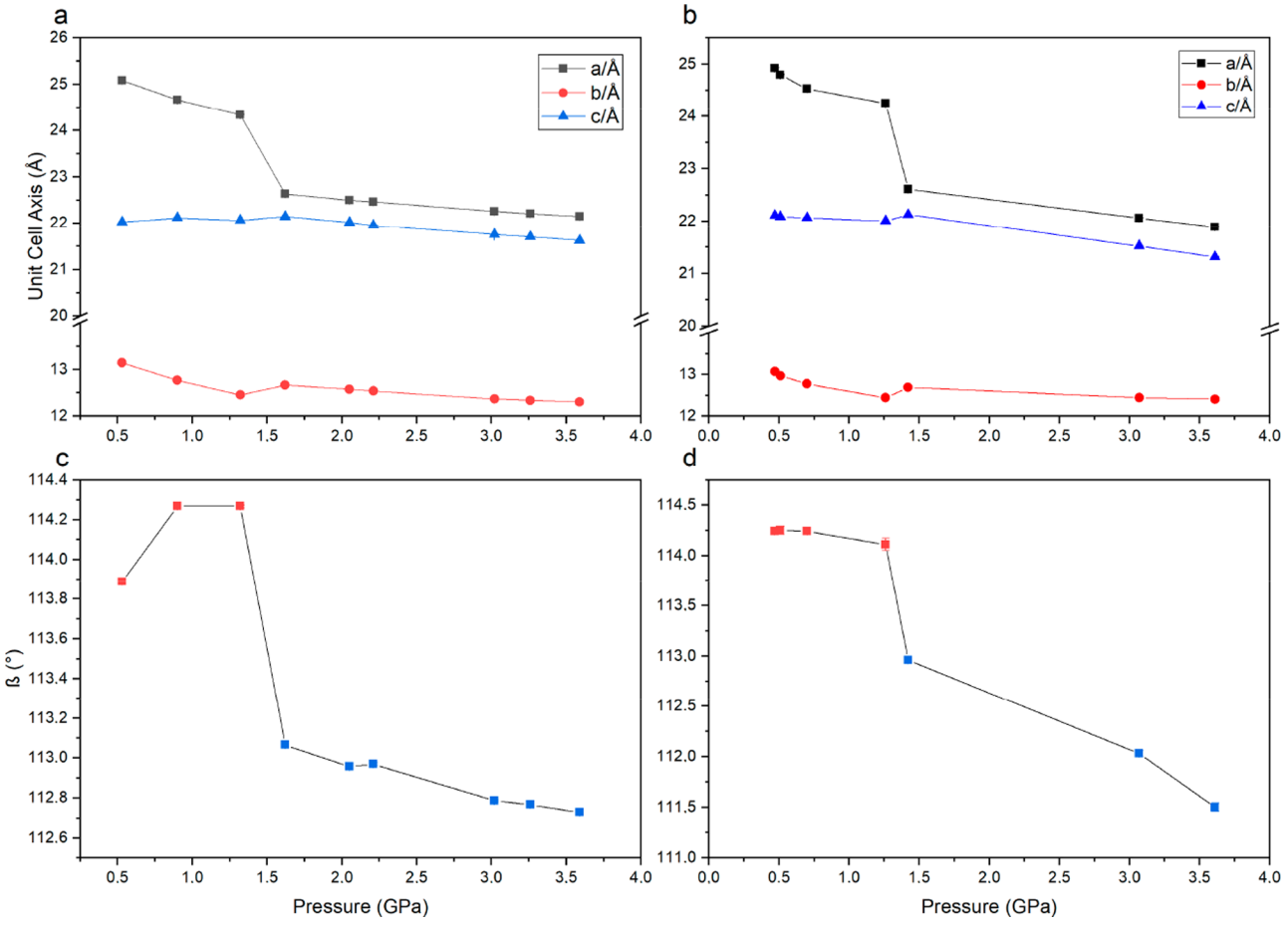

Figure 2. (a, b) shows the unit cell axes of **1Dy** (a) and **1Ho** (b) as a function of pressure. Black squares, red circles, and blue triangles represent the length of *a*-, *b*-, and *c*-axes, respectively. (c, d) shows the unit cell angle β of **1Dy** (c) and **1Ho** (d) as a function of pressure. The data is colored according to the phases, with red being phase 2 and blue being phase 3. Lines are added as visual guides.

suite,[22] using the UB3LYP[23,24] functional. We have substituted Dy by Gd to simplify the calculations. The CSDZ (Cundari Stevens Double Zeta)[25] and SDD (Stuttgart–Dresden)[26−28] ECP (Effective Core Potential) along with their corresponding basis set was used for Gd and I atom, respectively. The 6-31G* basis set[29,30] was used for the rest of the elements.

DOI: 10.1021/acs.inorgchem.9b02962
Inorg. Chem. 2020, 59, 717−729

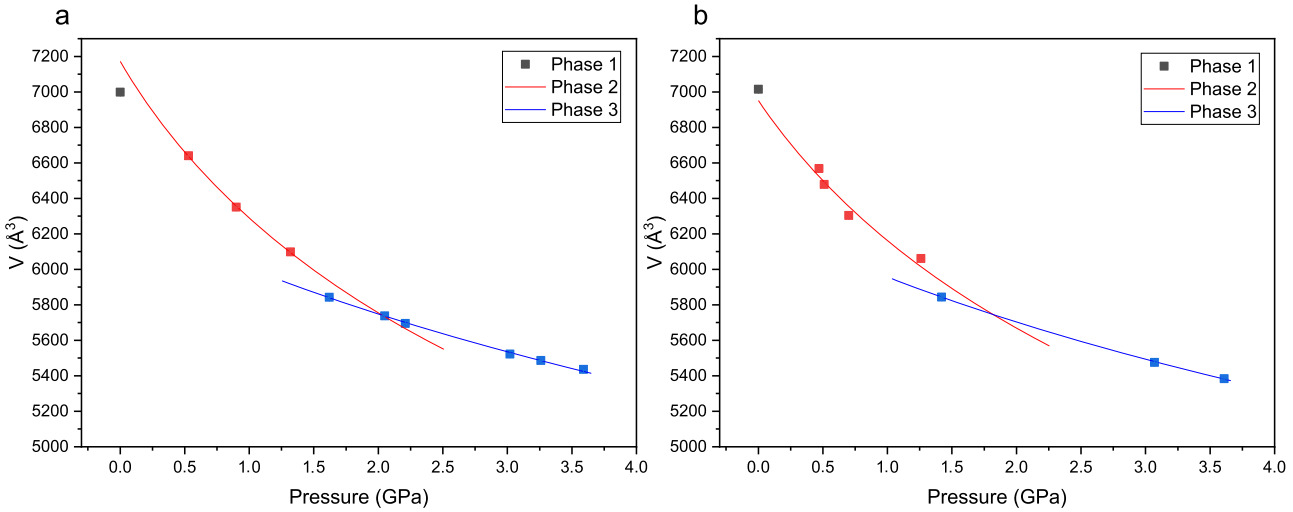

Figure 3. These figures show the unit cell volume (Z = 4) of **1Dy** (**a**) and **1Ho** (**b**) as a function of pressure. Phase 1 is indicated as black, phase 2 as red and phase 3 as blue squares. The squares are pressure points and the lines are second-order Birch−Murnaghan EoS fits for phase 2 and 3.

Ab initio calculations were performed on the optimized structures at ambient pressure as well as at all pressure points. The calculations were performed on the complex, including the solvents, counteranions that are shown earlier to play an important role in determining the U_{eff} values.[21,31] The calculations were made using MOLCAS 8.2[32−34] and were conducted with a multiconfigurational approach incorporating relativistic effects based on the Douglas−Kroll Hamiltonian.[32] The disk space has been reduced by the Cholesky decomposition technique.[32,33,35−41] ANO-RCC basis set were used for all atoms. The following contraction schemes were used: [8s7p5d3f2g1h] for Dy and Ho, [7s6p4d2f1g] for I, [3s2p] for N, [3s2p1d.] for O, [4s3p] for P, [3s2p] for C, and [2s] for H. The ground-state atomic multiplicity is $^6H_{15/2}$ for Dy(III), while it is $^5I_8$ for Ho(III).

Complete active space self-consistent field (CASSCF) calculations were performed with the active space containing nine active electrons in seven active orbitals (CAS(9,7)) for **1Dy**. With this active space, 21 sextet states were computed. To obtain the spin−orbit coupled states these CASSCF computed spin-free states (only 21 sextets were considered) were mixed via the RASSI-SO (restricted active space state interaction with spin−orbit coupling) module.[42] Finally, the energies of the lowest lying states, *g*-tensors, and crystal-field (CF) parameters were computed using the SINGLE_ANISO module.[33]

The CASSCF calculations for **1Ho** were performed with ten active electrons in seven active orbitals (CAS(10,7)). With this active space, 35 quintet, 210 triplet, and 196 singlet states were computed. To obtain the spin−orbit states, these CASSCF computed spin-free states were mixed via the RASSI-SO module.

RESULTS AND DISCUSSION

Ambient Pressure Crystal Structures. At ambient pressure,[3,21] both compounds crystallize in the triclinic space group $P\bar{1}$. The unit cell volumes are close to 3500 Å^3 and contain two formula units. One formula unit consists of one lanthanide ion, two coordinated phosphonic diamide ligands, five coordinated water molecules, three iodides, and two free phosphonic diamide ligands, which all form hydrogen bonds with the water molecules of the complex, and then finally it also includes one lattice water molecule (see Figure 1). All the complexes in the unit cells are aligned parallel. Selected crystallographic data are given in Tables 1 and 2, while further details may be found in the Supporting Information.

The two compounds are isostructural at room temperature. The lanthanide ion interacts stronger with the axial ligands with bond lengths of approximately 2.2 Å, while the bond lengths to the equatorial water molecules are approximately 2.4 Å. At ambient pressure, the Ln-ion is bound almost linearly to the phosphonic diamide ligands with an O−Ln−O angle of approximately 175°. The shortest Ln−Ln distance at ambient pressure is 10.840 Å for **1Dy** and 10.845 Å for **1Ho**, suggesting that the intermolecular magnetic interactions are small.

High-Pressure Crystal Structures. When gradually applying pressure, both compounds undergo two phase transitions at very similar pressures. We denote the ambient-pressure crystal structure as phase 1, and we observe phase 2 already at the very first pressure point (~0.5 GPa) for both compounds. Several attempts to reach a lower pressure in order to determine more precisely the phase transition pressure were not successful. In phase 2, the compounds have the monoclinic space group $I2/a$, and the unit cell volume has doubled, now containing four formula units, with only half the complex in the asymmetric unit. When the pressure is increased above 1.4 GPa, phase 3 appears in space group $P2_1/c$. The changes of the unit cell dimensions with pressure are highly similar for **1Dy** and **1Ho** (see Figure 2). The decrease for the *b*- and *c*-axes is generally small (less than 1.0 Å over the full pressure range), while it is larger for the *a*-axis, especially related to the second phase transition. The β-angle changes strongly during the second phase transition, while also generally decreasing. The ambient-pressure structure is triclinic, and we can therefore only compare the volumes, not the individual unit cell dimensions.

The decrease in unit cell volume as a function of pressure is shown in Figure 3 where the points are colored according to the three phases. In these figures, second order Birch−Murnaghan[43] Equation of State fits (EoS fits) are shown as full lines.[44] It should be noted that the precision of the fitted parameters suffers from the low number of points for each phase, but they can nevertheless still be used to highlight the changes between phases. The EoS lines show a clear change in curvature and thus compressibility between the phases.[45] This is quantified in terms of the refined bulk modulus K_0, which in phase 2 for both compounds is ~6 GPa, while it is ~17 GPa for phase 3 (see Table 3). We interpret the strong resemblance of the values as a sign of high precision of the high-pressure structural results.

DOI: 10.1021/acs.inorgchem.9b02962
Inorg. Chem. 2020, 59, 717−729

Table 3. Bulk Modulus K_0 (GPa) for Phases 2 and 3 of 1Dy and 1Ho

	1Dy	1Ho
phase 2	5.85	6.52
phase 3	17.1	17.3

Since the symmetry around the central ion undoubtedly has a strong influence on the magnetic anisotropy of the molecule, it is relevant to investigate in more detail how the geometry changes with pressure. At ambient pressure, the angle between the axial ligands (O−Ln−O) is 175°. For **1Ho**, this angle decreases with pressure especially in phase 2 from 172 to 167° between 0.5 and 0.7 GPa, while in phase 3 it is almost constant (see Figure 4). The same tendencies for each phase are not discernible in **1Dy**. Here, there is a large increase in the angle at the last point of phase 2 (1.32 GPa) followed by a significant decrease upon changing to phase 3. In contrast, the bond distances involving Dy and Ho only change slightly (Figure S1).

Instead of focusing on individual bonds to describe the structure, we may instead use continuous shape measures calculated with the program SHAPE[46] to quantify how much the symmetry of the complexes deviate from perfect pentagonal bipyramidal (D_{5h}) at different pressures, thus taking into account also the distribution of the equatorial ligands. For both compounds, the complex is closest to the perfect shape at ambient pressure (Figure 5). In general, the shape of the first coordination sphere deviates more from the ideal polyhedron with increasing pressure, but for **1Ho** the shape measure decreases between 0.7 and 3.07 GPa before it increases again for the last pressure point. For **1Dy**, it can be seen that the third pressure point of phase 2 (1.32 GPa) has a significantly decreased shape measure, and thus reveal a structure closer to an idealized coordination sphere. This obviously correlates well with the observation of a significant increase in the axial angle at this specific pressure point (Figure 4a).

If we look beyond the first coordination sphere, then we first find three iodide ions and two free phosphonamide ligands which all form hydrogen bonds to two of the five equatorial water molecules (Figure S2). The distance between these iodides and the central metal ion changes from ca. 5.0 to 4.8 Å over the measured pressure range, with I2 being closer to the Ln than I1 and I3 in phases 1 and 2. In contrast, I1 and I3 remain equidistant from Ln in the full pressure range, i.e., in all crystalline phases observed. In phase 3, the distance to all three iodides is almost equal for **1Ho**, while I2 remains slightly closer in **1Dy**. The distance from the coordinating oxygen in the two free ligands to the nearest Ln is approximately 4.1 Å and decreases only slightly with pressure. For **1Ho**, the distance to the two ligands is very similar at all pressures, while for **1Dy** there is a significant unexplained difference at 2.21 GPa. The distance is steadily decreasing with pressure for **1Ho**, while it varies more randomly in **1Dy**.

High-Pressure Magnetic Properties. As mentioned in the introduction, a strong motivation for us is to examine the magneto-structural correlations. We have therefore performed direct-current (dc) measurements of the field dependence of the magnetization on powder crystalline samples of **1Dy** and **1Ho** inside a pressure cell. Because of the limits of the used pressure cell, experimental high-pressure data was only measured up to a limit of around 1.0 GPa. It is necessary at this stage to point out that the high-pressure magnetic measurements were carried out at very low temperature, while the high-pressure crystal structures were determined at room temperature. It is exceedingly difficult to perform high-pressure crystallography at extremely low temperatures ($T > 2$ K), and we therefore in this work assume that the room-temperature ambient-pressure crystal structure remains the same down to 4 K and that the trends observed in the structural evolution with pressure at room temperature is mirrored at low temperature. However, we can obviously not be certain that the phase transitions also occur at the lowest temperatures. We are currently constructing a lab diffractometer, which will allow us to combine the use of specially designed miniature high-pressure cells inside a three-stage closed-cycle cryostat, expanding the attainable P, T phase space to $P > 10$ GPa and $T > 3$ K, and these compounds will be interesting to examine when this is operational.

Figure 6 shows the hysteresis loops measured for **1Dy** at different applied pressures and temperatures, all measured with

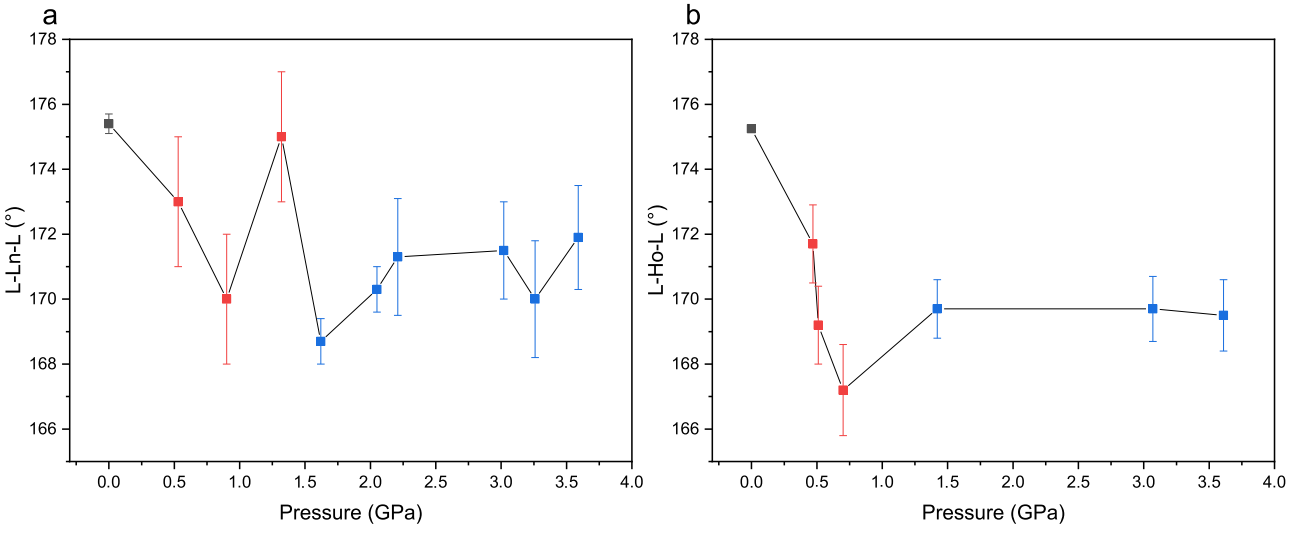

Figure 4. (a, b) Angle between the lanthanide ion and the axial ligands. Black, red, and blue squares represent phases 1−3, respectively. (a) **1Dy** and (b) **1Ho**. Lines are added as visual guides. The large error bars reflect the uncertainty of the atomic positions from a high-pressure experiment.

DOI: 10.1021/acs.inorgchem.9b02962
Inorg. Chem. 2020, 59, 717−729

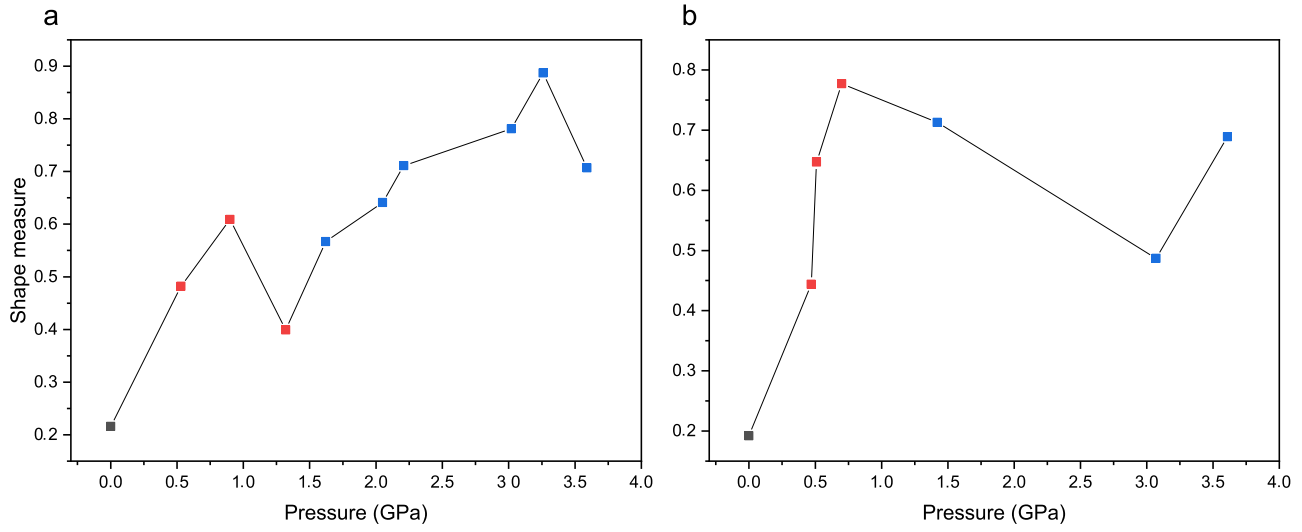

Figure 5. Shape measures (D_{5h}) of **1Dy** (a) and **1Ho** (b). Points are colored according to the phases, and lines are drawn as visual guides.

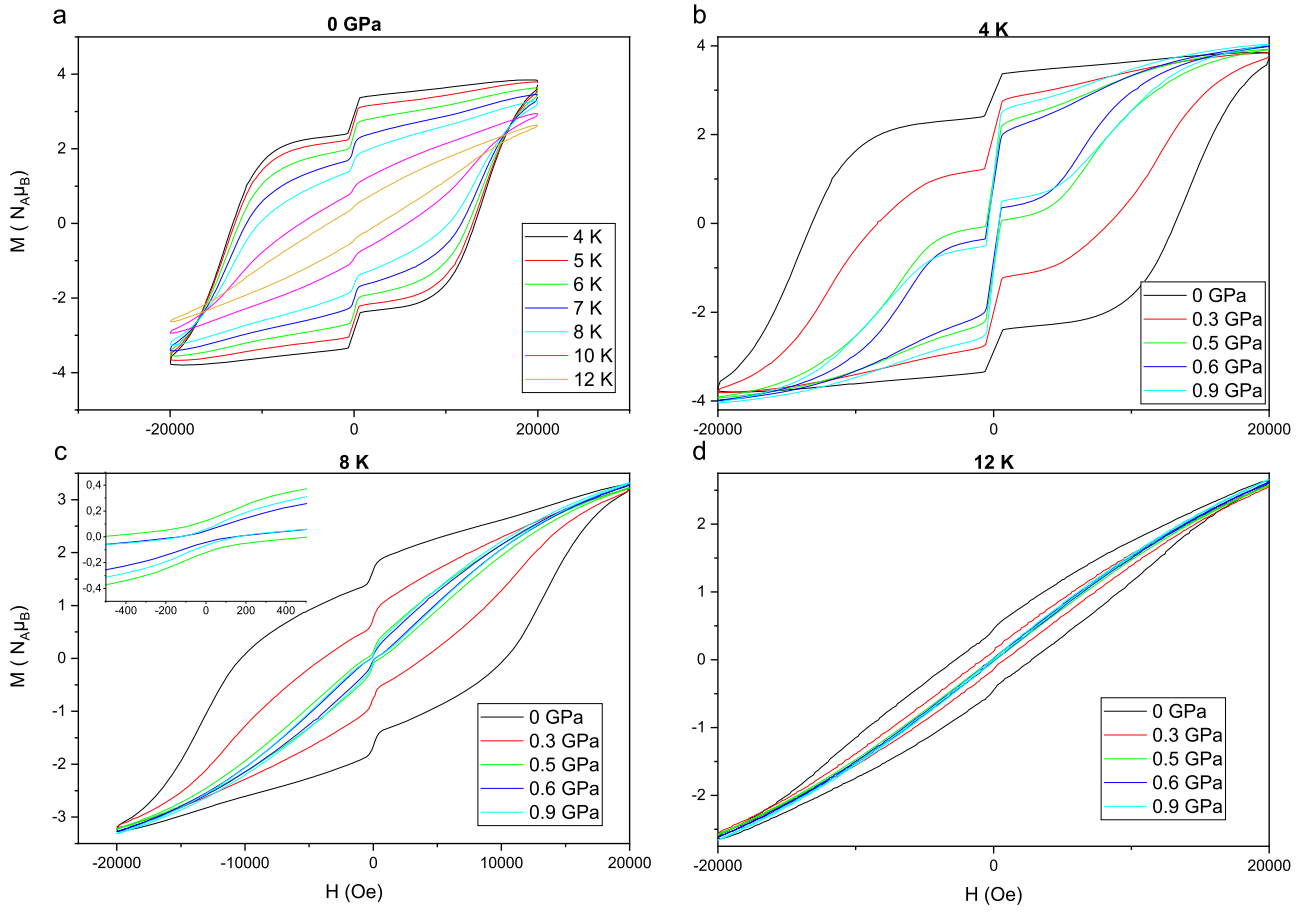

Figure 6. These figures show the hysteresis loops for **1Dy**. (a) Hysteresis loops at 0 GPa and different temperatures between 4 and 12 K. (b–d) Hysteresis loops for 4 (b), 8 (c) and 12 K (d) at five different pressures (0 GPa: black, 0.3 GPa: red, 0.5 GPa: green, 0.6 GPa: blue, and 0.9 GPa: cyan).

the sample inside a pressure cell. All data was measured using a sweep rate of 100 Oe/s. Figure 6a shows the temperature dependence of the hysteresis loops at ambient pressure in the interval 4–12 K. With this sweep rate and at ambient pressure the hysteresis loops are still open at 12 K. Figure 6b–d shows the pressure dependence of the hysteresis loops at fixed temperatures of 4, 8, and 12 K, respectively. At each temperature, hysteresis loops were measured at 5 different pressures in the interval 0–0.9 GPa. At 4 K, the hysteresis loops are still open at the highest pressure of 0.9 GPa. The inset in Figure 6c shows that there is still a small opening in the hysteresis loops at 8 K and pressures above 0.3 GPa. At 12 K, only the loops measured at 0 and 0.3 GPa show significant opening.

DOI: 10.1021/acs.inorgchem.9b02962
Inorg. Chem. 2020, 59, 717–729

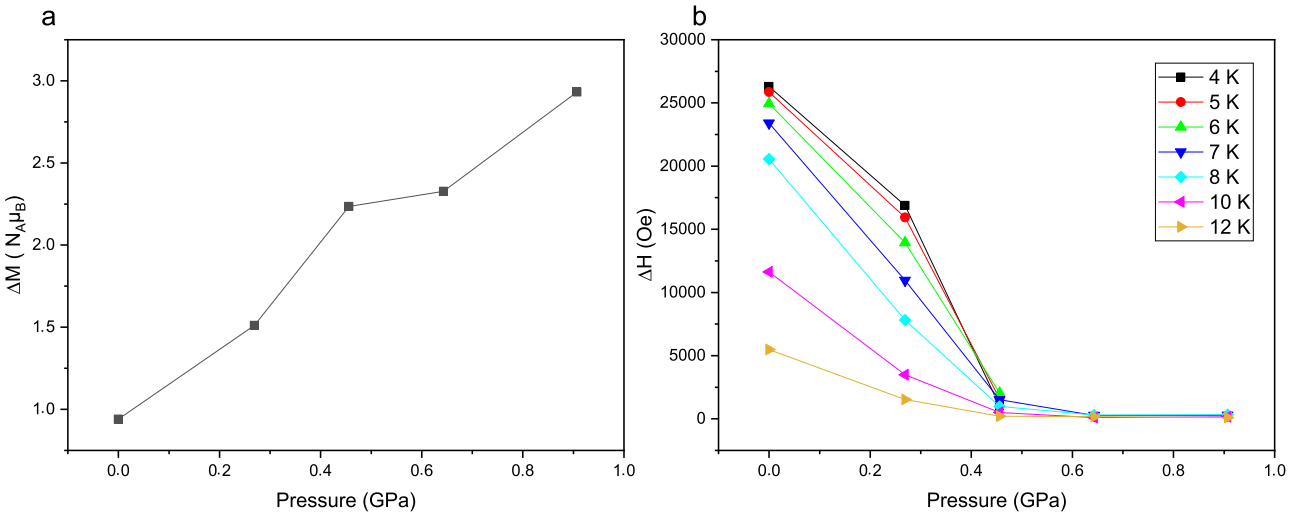

Figure 7. (a) Size of the steps of the **1Dy** 4 K hysteresis curves at different pressures. (b) Width of the **1Dy** hysteresis loops at $M = 0$ as a function of pressure and at different temperatures. Lines are added as visual guides.

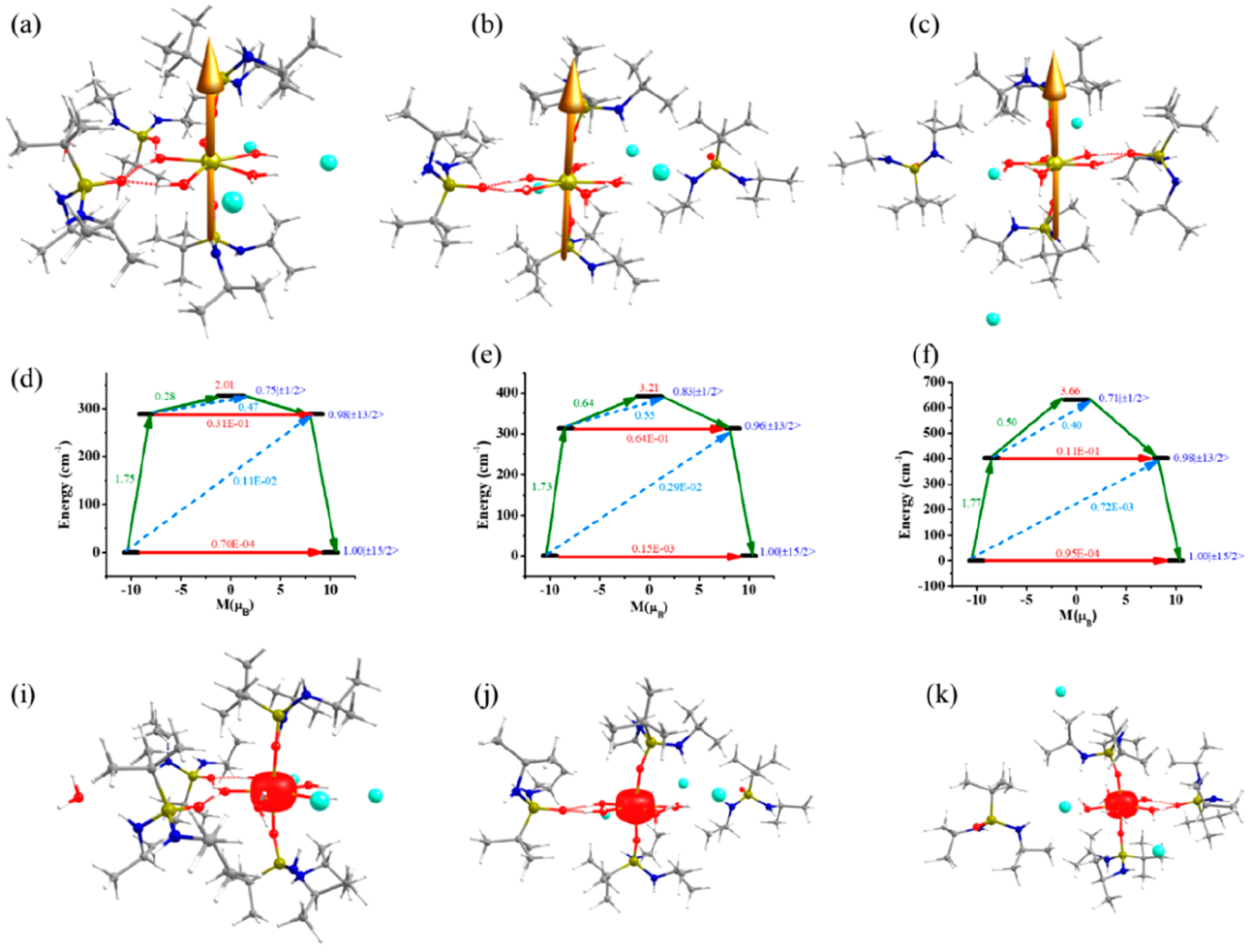

Figure 8. Anisotropy axis of **1Dy** at (a) 0 GPa (b) 2.05 GPa (c) 3.59 GPa. Color code: Dy, greenish-yellow; I, cyan; P, light yellow; O, red; N, blue; C, gray; H, white. The mechanism of magnetic relaxation of **1Dy** at (d) 0 GPa (e) 2.05 GPa (f) 3.59 GPa. The red line represents QTM via ground states and TA-QTM via excited states. The dashed sky blue line indicates a possible Orbach process. The olive line indicates possible pathways of magnetic relaxation. The blue characters indicate the m_J composition of the Kramers doublet (KD) derived from $^6H_{15/2}$ ground state. Beta electron density of **1Dy** at (i) 0 GPa, (j) 2.05 GPa, and (k) 3.59 GPa.

The hysteresis loops for **1Dy** (Figure 6) show clear steps in the magnetization at zero-field, which is a clear indicator of QTM. It is not uncommon for Dy(III) SMMs to have steps in their hysteresis loops.[47] It is evident, especially from Figure 6b,

DOI: 10.1021/acs.inorgchem.9b02962
Inorg. Chem. 2020, 59, 717−729

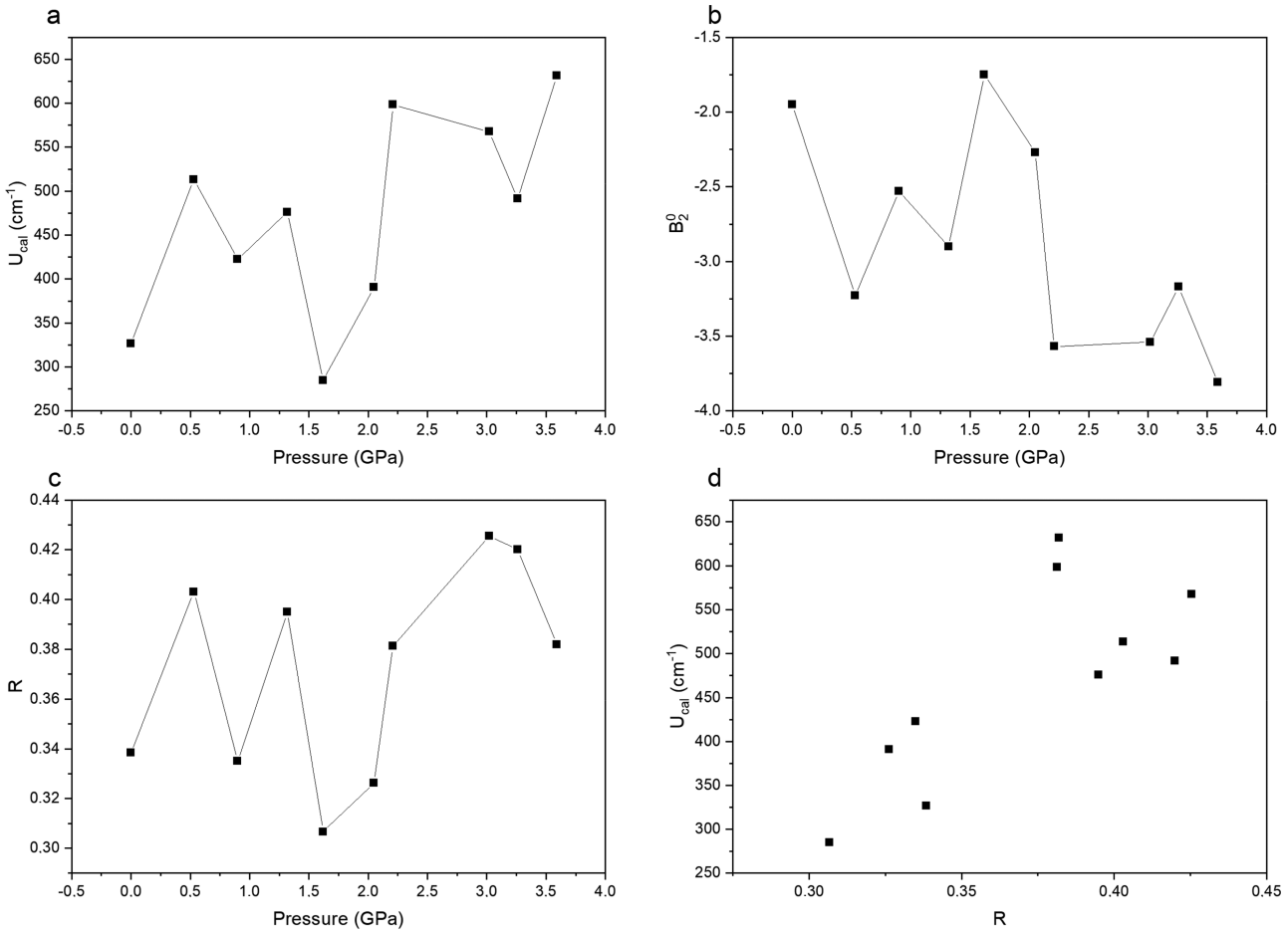

Figure 9. Selected parameters as a function of pressure in **1Dy**. (a) The estimated energy barrier, (b) the axial CFP (B_2^0) value, (c) R. (d) shows U_{cal} versus R.

that the steps increase in size with increasing pressure (see also Figure 7a, where the extracted step size is shown as a function of pressure) indicating that the extent of tunneling increases with pressure. This can be explained by a distortion of the symmetry around the Dy(III) ion with increasing pressure which is consistent with the X-ray data.

To further evaluate the influence of pressure on the size of the hysteresis loop opening, Figure 7b shows the total width of the loops at $M = 0$ at different temperatures and pressures. At ambient pressure, we observe a strong decline in the width with increasing temperature. A similar dependency on the temperature is apparent in the data measured at 0.3 GPa, which strongly suggests that at a pressure of 0.3 GPa, **1Dy** still exhibits SMM character. At 0.5 GPa, we only observe a small loop opening even at the lowest temperature, and this quickly disappears as the temperature is increased. At pressures higher than 0.5 GPa, no significant opening in the hysteresis loops is seen, which means that such pressures are sufficient to quench the blocking of magnetization under the given measuring conditions. However, the nonzero opening observed at 0.3 GPa tells us that the SMM properties of **1Dy** are stable under relatively small pressures. At room temperature, we have established that the phase transition from phase 1 to 2 occurs at pressures below 0.5 GPa, but whether or not it has taken place at 0.3 GPa is unknown. One interpretation of the pressure-dependent magnetic measurements could be, given the persistence of the loop opening at 0.3 GPa, that this pressure is below the phase transition. However, as mentioned previously, we have no certainty for the presence of phase transitions at these low temperatures. In addition, we do not see any strong discontinuities in the derived structural properties at the phase transitions at room temperature that would make us predict that the magnetic properties should change fundamentally concomitantly with the phase changes. Overall, the structural consequence of increasing the pressure is a distortion away from ideal symmetry, which will, all else equal, lead to increased tunneling rates.

Theoretical Studies. In an attempt to study the relaxation mechanism and how they are influenced by pressure, we have carried out *ab initio* CASSCF/RASSI-SO/SINGLE_ANISO calculations on the X-ray structure of a **1Dy** molecule at different pressure points where the H atom positions are optimized using DFT methods (see the "Computational Details" section for more information).

Ambient Pressure. The calculation on the structure at ambient pressure reveals an axial *g*-tensor ($g_x = g_y = 0.000$, $g_z = 19.973$) in the ground state which leads to very small quantum tunnelling of magnetization (QTM) (Table S3). The anisotropy axis is oriented along the axial O−Dy−O bond (shown in Figure 8a), and the Kramers doublets (KDs) generated from the $^6H_{15/2}$ state span up to 596.5 cm^{-1} (Table S3). The QTM in the second excited state becomes large enough for magnetization reversal (Figure 8d−f), which means that the calculated energy barrier to magnetic relaxation,

DOI: 10.1021/acs.inorgchem.9b02962
Inorg. Chem. 2020, 59, 717−729

denoted U_{cal}, attains a value of 326.5 cm^{-1}. This value deviates from our previous report (478 cm^{-1}) which could be attributed to the difference in the temperatures of crystal structure determination (in this study performed at room temperature, while previous study used X-ray data measured at 120 K).[21]

The axiality of the CF may be quantified by examining the atomic charges of the ligands. Here we implement the LoProp charge analysis,[48] which reveals significantly larger negative charges on the axial oxygen atoms (ca. −1.15e) than on the equatorial oxygen atoms (ca. −0.8e) (see Table S4). This will stabilize the $m_J = |\pm 15/2\rangle$ state as the ground state, as this has a distinctly oblate 4f electron density distribution, in contrast to other m_J-states. This oblateness is directly illustrated by the calculated β-electron density (Figure 8g−i) using the procedure of Ruiz et al.[49] In an analogous manner, we can also use the CF parameters (CFPs) which have been estimated using Stevens formalism $H_{CF} = \sum_{k=2,4,6}\sum_{q=-k}^{k} B_k^q \tilde{O}_k^q$, where B_k^q and $\tilde{O}_k^q$ are the CFPs and Stevens operators, respectively,[50] to show the magnetic anisotropy. QTM becomes smaller when the axial CFPs B_k^q ($q = 0$) becomes larger compared to the nonaxial B_k^q ($q \neq 0$) CFPs. The large and negative axial CFPs implies strong axiality of the **1Dy** at ambient pressure and stabilization of large m_J ($\pm 15/2$) as the ground state (Table S5).

High Pressures. Calculations show that the anisotropy axis is found to be oriented along the axial O−Dy−O direction in the ground state at all pressure points (Figures 8 and S5). The angle between the anisotropy axis of KD1 and KD2 of **1Dy** is found to be very small (less than 10°) for all pressures except 1.62 GPa, where it is 13.2° (Table S6).

It is possible to derive a geometrical parameter which combines the angular deviation from linearity of the O−M−O part with the bond distance asymmetry between axial and equatorial bonds and produces one single number, which we denote R (for details, see the Supporting Information). This number, R, correlates positively with the energy barrier, U_{cal}, as shown for **1Dy** in Figure 9d and for **1Ho** in Figure 11.

At the first pressure point (0.53 GPa), the splitting of the KDs is found to increase. As was the case at ambient pressure, significant transverse anisotropy appears in the second excited KD which implies relaxation of magnetization at this level and leads to a U_{cal} of 513.4 cm^{-1} (Table S4). As the pressure is increased further to 0.90 GPa, the geometrical parameter R drops substantially, and this is mirrored in a decrease in both the U_{cal} value (422.6 cm^{-1}) and the energy splitting of the eight KDs (Table S3 and Figure S6). Increasing the pressure to 1.32 GPa enlarges the geometrical distortion (larger R) which is accompanied by larger U_{cal} and B_2^0. The pressure-induced geometrical variations of the first coordination sphere in **1Dy**, which are combined in the value of R, generally describe the variations in the energy barrier quite well. However, even though we use a rather simplified explanation, we are aware that other factors influence the energy levels. For instance, the inclusion of neighboring ions in the calculations is shown in the next section to have a profound effect. Similarly, the spatial distribution of iodide ions and the hydrogen bonding solvent molecules around the central molecule will to some extent influence the electronic wave function. These latter effects have not been examined in this work.

Figure 10 shows that the m_J-states $|\pm 15/2\rangle$, $|\pm 13/2\rangle$, and $|\pm 1/2\rangle$ are the ground, first, and second excited states, respectively at all pressure points. The order of the other excited states is found to vary as the pressure is changed.

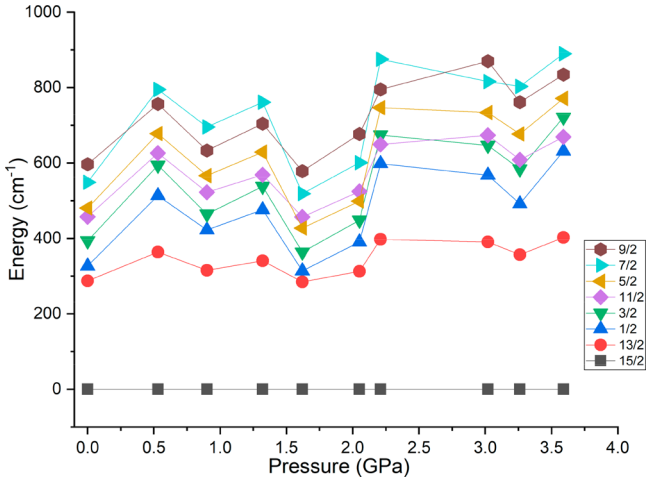

Figure 10. Energy splitting of the eight KDs of **1Dy** along with the change of m_J level at various pressure points.

The above calculations are carried out on single molecules including the nearest counterions and solvent molecules. However, neighboring molecules at longer separations may also influence the magnetic properties not only when the magnetic ions are close enough to allow magnetic exchange interactions. This has been found to influence the magnetic anisotropy in some cases,[51] while in other cases no noticeable differences are detected.[52] One can argue that this is particularly important for high-pressure studies, as the intermolecular distances are altered in a complicated manner, and it is important to check the role of intermolecular interactions in the magnetization relaxation. To take this effect into account, we have calculated atomic charges for the six closest ions and molecules surrounding a central moiety using a point charge model with CASSCF-computed LoProp charges, and in this way perturbed the electronic structure calculation.[52−55]

The calculation reveals changes in the U_{cal} value (46 cm^{-1}) and the overall CF splitting (32 cm^{-1}) at 0 GPa (Figure S8 and Table S7). At the highest pressure of 3.59 GPa, the U_{cal} value has increased from 631.4 to 676.0 cm^{-1} and the overall splitting has increased from 889.5 to 1382.8 cm^{-1}, clearly revealing significance of secondary atoms on the local CFs (Figure S9 and Table S7), an effect that is often ignored. The exact relationship between U_{cal} and external pressure is, however, complicated. Generally, atoms approach each other when the pressure is increased and the electrostatic field increases, but the resulting compression of the crystal structure is not isotropic (although the applied pressure is isotropic if hydrostatic conditions are met) which means that the field is anisotropic. In these crystal structures we find that the phase changes have the conspicuous effect that the shortest Dy···Dy distance is actually increasing, not decreasing, with increasing pressure.

The change in the LoProp charge and axial CFP are significant when the intermolecular interaction has been included in our calculations (Tables S9 and S10). These calculations clearly reveal that intermolecular effects related to Madelung constants, that are often ignored,[52] are necessary if such static pressures are applied as substantial changes to the estimated energy barrier, g-anisotropy and overall CF splittings

DOI: 10.1021/acs.inorgchem.9b02962
Inorg. Chem. 2020, 59, 717−729

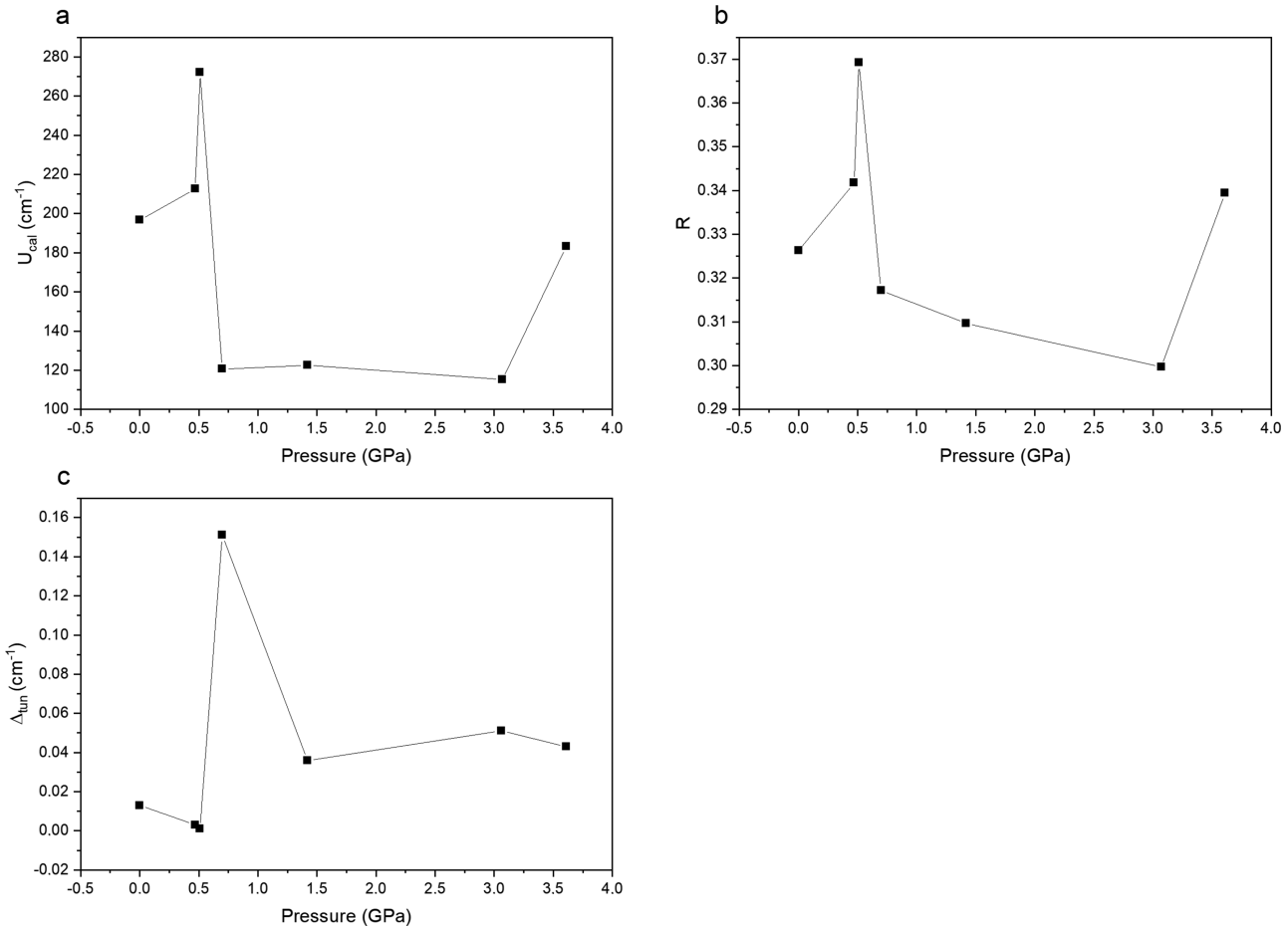

Figure 11. Pressure dependence of (a) the estimated energy gap between the ground and first excited pseudo doublet state of **1Ho**, (b) the value of the geometrical parameter *R*, and (c) the tunnel splitting between the pseudo-KDs of **1Ho**.

are noticeable even with a simpler model that is chosen to represent the lattice effect.

In the case of **1Ho** at ambient pressure, the ground state pseudodoublet possesses a g_{zz} value of 19.84 which is close to the limiting, purely axial value of 20 (Table S11). The axial nature of the ground-state pseudodoublet leads to the very small tunnel splitting (Δ_{tun}) of 0.013 cm^{-1} which results in the stabilization of $|m_J = \pm 8\rangle$ as the ground state (Table S11). For the same reasons as explained for **1Dy**, the LoProp charges in **1Ho** imply stabilization of large m_J as ground state (Table S12 and Figure S4). The tunnel splitting between the first excited pseudodoublets becomes significant (0.764 cm^{-1}) for the relaxation of magnetization. This leads to the U_{cal} value of 196.7 cm^{-1} which is the difference of energy between ground and first excited pseudo doublets. The deviation of this U_{cal} value from the previously calculated energy barrier by Murugavel et al. is due to the small structural difference and optimized position of hydrogen in our calculation.[3]

As the pressure is increased to 0.47 GPa, the value of *R* increases due primarily to shortening of the axial Ho−O bond distance and Δ_{tun} in the ground-state pseudodoublet decreases. The pressure increase leads to the enhancement of U_{cal} value to 212.5 cm^{-1} (Table S11). Further increase in pressure at 0.51 GPa leads to the very small Δ_{tun} (0.001 cm^{-1}) between the ground-state pseudodoublets. As for the 0.47 GPa structure, Δ_{tun} in the first excited pseudodoublet becomes very large (2.480) and leads to a U_{cal} value of 272.2 cm^{-1} (Table S11).

In general, we find for **1Ho** that large *R*-values result in substantial U_{cal} values (Figure 11). Similarly, the low value of *R* (0.38) found at 0.70 GPa is accompanied by the largest Δ_{tun} between the ground state pseudodoublets (0.151 cm^{-1}). At this pressure point, the large deviation of the axial O−Ho−O angle from 180° is the main reason for the small *R* value, and this coincides with a significant decrease in the LoProp charges of the axial oxygen atoms (ca. −1.09 compared to ca. −1.12 at all other pressures, see also Table S12). Importantly, the relaxation will at this pressure occur in the ground state resulting in the absence of zero-field SIM behavior. The tunnel splitting remains significant for all subsequent pressures and direct QTM in the ground-state pseudodoublet takes place (Figure 11c).

CONCLUSIONS

In conclusion, the crystal structure of two air-stable isostructural Dy(III) and Ho(III) SMMs with pseudo-D_{5h} symmetry was investigated at pressures between 0 and 3.6 GPa. The structural investigations revealed two phase transitions for both compounds: one just above ambient pressure (~0.5 GPa) from the triclinic space group $P\bar{1}$ to the monoclinic space group *I*2/*a* and another transition close to 1.4 GPa to the monoclinic space group $P2_1/c$. Overall, the results revealed a generally increasing deformation of the D_{5h} symmetry around the lanthanide ions upon increasing pressure. The dc magnetic measurements of **1Dy** showed

DOI: 10.1021/acs.inorgchem.9b02962
Inorg. Chem. 2020, 59, 717−729

steps in the hysteresis loops indicating quantum tunnelling of magnetization (QTM). Measurements performed under increasing pressure showed an increase in the magnitude of these steps indicating an increase in QTM with pressure. This is consistent with the decrease in the symmetry around the ion with increasing pressure, which would lead to QTM. The measurements also showed that the SMM properties of **1Dy** were somewhat stable at lower pressures. *Ab initio* calculations have been used to show how the energy barrier to magnetic relaxation, U_{cal}, changes with pressure. For **1Dy**, U_{cal} fluctuates strongly but overall increases with pressure, while the situation is the opposite for **1Ho**, where U_{cal} is generally lower at higher pressures than at ambient conditions. There are many structural parameters such as O−M−O (M = Ho and Dy) angles, M−ligand distances, M−solvent distances, and M−counteranion distances that may be playing their part in controlling the calculated barrier height. Interestingly, we find that the value of U_{cal} is correlated with a geometrical parameter *R*, which is defined as a combination of O−M−O angle and M−O distances. We also find that the intermolecular interactions, included by a point-charge model, have a large effect on the electronic energy levels, particularly at higher hydrostatic pressure where the secondary coordination sphere of ions and molecules is most strongly perturbed by pressure.

■ ASSOCIATED CONTENT

Supporting Information

The Supporting Information is available free of charge at https://pubs.acs.org/doi/10.1021/acs.inorgchem.9b02962.

Detailed structural results, magnetization curves for **1Ho** at various pressures and temperatures (PDF)

Accession Codes

CCDC 1906576−1906592 contain the supplementary crystallographic data for this paper. These data can be obtained free of charge via www.ccdc.cam.ac.uk/data_request/cif, or by emailing data_request@ccdc.cam.ac.uk, or by contacting The Cambridge Crystallographic Data Centre, 12 Union Road, Cambridge CB2 1EZ, UK; fax: +44 1223 336033.

■ AUTHOR INFORMATION

Corresponding Author

*E-mail: jacobo@chem.au.dk.

ORCID

Gopalan Rajaraman: 0000-0001-6133-3026

Jacob Overgaard: 0000-0001-6492-7962

Funding

Danish National Research Foundation.

Notes

The authors declare no competing financial interest.

■ ACKNOWLEDGMENTS

We acknowledge the Danish National Research Foundation for financial support (DNRF-93). R.M. thanks the SERB, New Delhi, for support through a J. C. Bose Fellowship. S.D. thanks to UGC for SRF fellowship. G.R. thanks the Science and Engineering Research Board (CRG/2018/000430) New Delhi, for financial support of this research. The computational facility at Indian Institute of Technology Bombay is greatly acknowledged.

■ REFERENCES

(1) Sessoli, R.; Tsai, H. L.; Schake, A. R.; Wang, S.; Vincent, J. B.; Folting, K.; Gatteschi, D.; Christou, G.; Hendrickson, D. N. High-spin molecules: [Mn12O12(O2CR)16(H2O)4]. *J. Am. Chem. Soc.* **1993**, *115* (5), 1804−1816.

(2) Sessoli, R.; Gatteschi, D.; Caneschi, A.; Novak, M. A. Magnetic bistability in a metal-ion cluster. *Nature* **1993**, *365*, 141.

(3) Gupta, S. K.; Rajeshkumar, T.; Rajaraman, G.; Murugavel, R. Is a strong axial crystal-field the only essential condition for a large magnetic anisotropy barrier? The case of non-Kramers Ho(iii) versus Tb(iii). *Dalton Transactions* **2018**, *47* (2), 357−366.

(4) Ishikawa, N.; Sugita, M.; Ishikawa, T.; Koshihara, S.-y.; Kaizu, Y. Lanthanide Double-Decker Complexes Functioning as Magnets at the Single-Molecular Level. *J. Am. Chem. Soc.* **2003**, *125* (29), 8694−8695.

(5) Gupta, S. K.; Murugavel, R. Enriching lanthanide single-ion magnetism through symmetry and axiality. *Chem. Commun.* **2018**, *54* (30), 3685−3696.

(6) Guo, F.-S.; Day, B. M.; Chen, Y.-C.; Tong, M.-L.; Mansikkamaki, A.; Layfield, R. A. A Dysprosium Metallocene Single-Molecule Magnet Functioning at the Axial Limit. *Angew. Chem., Int. Ed.* **2017**, *56* (38), 11445−11449.

(7) Goodwin, C. A. P.; Ortu, F.; Reta, D.; Chilton, N. F.; Mills, D. P. Molecular magnetic hysteresis at 60 K in dysprosocenium. *Nature* **2017**, *548*, 439.

(8) Guo, F.-S.; Day, B. M.; Chen, Y.-C.; Tong, M.-L.; Mansikkamäki, A.; Layfield, R. A. Magnetic hysteresis up to 80 K in a dysprosium metallocene single-molecule magnet. *Science* **2018**, *362* (6421), 1400−1403.

(9) Gatteschi, D.; Sessoli, R.; Villain, J. *Molecular Nanomagnets*; OUP Oxford: 2006.

(10) Rinehart, J. D.; Long, J. R. Exploiting single-ion anisotropy in the design of f-element single-molecule magnets. *Chem. Sci.* **2011**, *2* (11), 2078−2085.

(11) Gregson, M.; Chilton, N. F.; Ariciu, A.-M.; Tuna, F.; Crowe, I. F.; Lewis, W.; Blake, A. J.; Collison, D.; McInnes, E. J. L.; Winpenny, R. E. P.; Liddle, S. T. A monometallic lanthanide bis(methanediide) single molecule magnet with a large energy barrier and complex spin relaxation behaviour. *Chem. Sci.* **2016**, *7* (1), 155−165.

(12) Chilton, N. F.; Goodwin, C. A. P.; Mills, D. P.; Winpenny, R. E. P. The first near-linear bis(amide) f-block complex: a blueprint for a high temperature single molecule magnet. *Chem. Commun.* **2015**, *51* (1), 101−103.

(13) Goodwin, C. A. P.; Ortu, F.; Reta, D.; Chilton, N. F.; Mills, D. P. Molecular magnetic hysteresis at 60 K in dysprosocenium. *Nature* **2017**, *548* (7668), 439−442.

(14) Mannini, M.; Sainctavit, P.; Sessoli, R.; Cartier dit Moulin, C.; Pineider, F.; Arrio, M.-A.; Cornia, A.; Gatteschi, D. XAS and XMCD Investigation of Mn12 Monolayers on Gold. *Chem. - Eur. J.* **2008**, *14* (25), 7530−7535.

(15) Prescimone, A.; Milios, C. J.; Moggach, S.; Warren, J. E.; Lennie, A. R.; Sanchez-Benitez, J.; Kamenev, K.; Bircher, R.; Murrie, M.; Parsons, S.; Brechin, E. K. [Mn6] under pressure: a combined crystallographic and magnetic study. *Angew. Chem., Int. Ed.* **2008**, *47* (15), 2828−31.

(16) Prescimone, A.; Sanchez-Benitez, J.; Kamenev, K. V.; Moggach, S. A.; Lennie, A. R.; Warren, J. E.; Murrie, M.; Parsons, S.; Brechin, E. K. High pressure effects on a trimetallic MnII/III SMM. *Dalton Transactions* **2009**, No. 36, 7390−7395.

(17) Craig, G. A.; Sarkar, A.; Woodall, C. H.; Hay, M. A.; Marriott, K. E. R.; Kamenev, K. V.; Moggach, S. A.; Brechin, E. K.; Parsons, S.; Rajaraman, G.; Murrie, M. Probing the origin of the giant magnetic anisotropy in trigonal bipyramidal Ni(ii) under high pressure. *Chemical Science* **2018**, *9* (6), 1551−1559.

(18) Gutlich, P.; Gaspar, A. B; Ksenofontov, V.; Garcia, Y. Pressure effect studies in molecular magnetism. *J. Phys.: Condens. Matter* **2004**, *16* (14), S1087.

(19) Craig, G. A.; Woodall, C. H.; McKellar, S. C.; Probert, M. R.; Kamenev, K. V.; Moggach, S. A.; Brechin, E. K.; Parsons, S.; Murrie,

DOI: 10.1021/acs.inorgchem.9b02962
Inorg. Chem. 2020, 59, 717−729

M. A high-pressure crystallographic and magnetic study of Na5[Mn(l-tart)2][middle dot]12H2O (l-tart = l-tartrate). *Dalton Transactions* **2015**, *44* (42), 18324−18328.
(20) Prescimone, A.; Milios, C. J.; Sanchez-Benitez, J.; Kamenev, K. V.; Loose, C.; Kortus, J.; Moggach, S.; Murrie, M.; Warren, J. E.; Lennie, A. R.; Parsons, S.; Brechin, E. K. High pressure induced spin changes and magneto-structural correlations in hexametallic SMMs. *Dalton Transactions* **2009**, No. 25, 4858−4867.
(21) Gupta, S. K.; Rajeshkumar, T.; Rajaraman, G.; Murugavel, R. An air-stable Dy(iii) single-ion magnet with high anisotropy barrier and blocking temperature. *Chemical Science* **2016**, *7* (8), 5181−5191.
(22) Frisch, M. J.; Trucks, G. W.; Schlegel, H. B.; Scuseria, G. E.; Robb, M. A.; Cheeseman, J. R.; Scalmani, G.; Barone, V.; Mennucci, B.; Petersson, G. A.; Nakatsuji, H.; Caricato, M.; Li, X.; Hratchian, H. P.; Izmaylov, A. F.; Bloino, J.; Zheng, G.; Sonnenberg, J. L.; Hada, M.; Ehara, M.; Toyota, K.; Fukuda, R.; Hasegawa, J.; Ishida, M.; Nakajima, T.; Honda, Y.; Kitao, O.; Nakai, H.; Vreven, T.; Montgomery, J. A., Jr.; Peralta, J. E.; Ogliaro, F.; Bearpark, M.; Heyd, J. J.; Brothers, E.; Kudin, K. N.; Staroverov, V. N.; Kobayashi, R.; Normand, J.; Raghavachari, K.; Rendell, A.; Burant, J. C.; Iyengar, S. S.; Tomasi, J.; Cossi, M.; Rega, N.; Millam, J. M.; Klene, M.; Knox, J. E.; Cross, J. B.; Bakken, V.; Adamo, C.; Jaramillo, J.; Gomperts, R.; Stratmann, R. E.; Yazyev, O.; Austin, A. J.; Cammi, R.; Pomelli, C.; Ochterski, J. W.; Martin, R. L.; Morokuma, K.; Zakrzewski, V. G.; Voth, G. A.; Salvador, P.; Dannenberg, J. J.; Dapprich, S.; Daniels, A. D.; Farkas, O.; Foresman, J. B.; Ortiz, J. V.; Cioslowski, J.; Fox, D. J. *Gaussian 09*, revision E.01; Gaussian, Inc.: Wallingford, CT, 2009.
(23) Becke, A. D. Density-Functional Thermochemistry 0.3. The Role of Exact Exchange. *J. Chem. Phys.* **1993**, *98* (7), 5648−5652.
(24) Lee, C. T.; Yang, W. T.; Parr, R. G. Development of the Colle-Salvetti Correlation-Energy Formula into a Functional of the Electron-Density. *Phys. Rev. B: Condens. Matter Mater. Phys.* **1988**, *37* (2), 785−789.
(25) Cundari, T. R.; Stevens, W. J. Effective core potential methods for the lanthanides. *J. Chem. Phys.* **1993**, *98* (7), 5555−5565.
(26) Cao, X.; Dolg, M. Segmented contraction scheme for small-core lanthanide pseudopotential basis sets. *J. Mol. Struct.: THEOCHEM* **2002**, *581* (1), 139−147.
(27) Cao, X.; Dolg, M. Valence basis sets for relativistic energy-consistent small-core lanthanide pseudopotentials. *J. Chem. Phys.* **2001**, *115* (16), 7348−7355.
(28) Dolg, M.; Stoll, H.; Preuss, H. A combination of quasirelativistic pseudopotential and ligand field calculations for lanthanoid compounds. *Theoret. Chim. Acta* **1993**, *85* (6), 441−450.
(29) Hariharan, P. C.; Pople, J. A. The influence of polarization functions on molecular orbital hydrogenation energies. *Theoret. Chim. Acta* **1973**, *28* (3), 213−222.
(30) Ditchfield, R.; Hehre, W. J.; Pople, J. A. Self-Consistent Molecular-Orbital Methods. IX. An Extended Gaussian-Type Basis for Molecular-Orbital Studies of Organic Molecules. *J. Chem. Phys.* **1971**, *54* (2), 724−728.
(31) Canaj, A. B.; Singh, M. K.; Regincós Marti, E.; Damjanović, M.; Wilson, C.; Céspedes, O.; Wernsdorfer, W.; Rajaraman, G.; Murrie, M. Boosting axiality in stable high-coordinate Dy(iii) single-molecule magnets. *Chem. Commun.* **2019**, *55*, 5950.
(32) Aquilante, F.; Autschbach, J.; Carlson, R. K.; Chibotaru, L. F.; Delcey, M. G.; De Vico, L.; Fdez. Galván, I.; Ferré, N.; Frutos, L. M.; Gagliardi, L.; et al. Molcas 8: New capabilities for multiconfigurational quantum chemical calculations across the periodic table. *J. Comput. Chem.* **2016**, *37* (5), 506−541.
(33) Chibotaru, L. F.; Ungur, L. Ab initio calculation of anisotropic magnetic properties of complexes. I. Unique definition of pseudospin Hamiltonians and their derivation. *J. Chem. Phys.* **2012**, *137* (6), 064112.
(34) Granovsky, A. A. Extended multi-configuration quasi-degenerate perturbation theory: The new approach to multi-state multi-reference perturbation theory. *J. Chem. Phys.* **2011**, *134* (21), 214113.
(35) Duncan, J. A. MOLCAS 7.2. *J. Am. Chem. Soc.* **2009**, *131* (6), 2416−2416.
(36) Aquilante, F.; De Vico, L.; Ferré, N.; Ghigo, G.; Malmqvist, P.-å.; Neogrády, P.; Pedersen, T. B.; Pitoňák, M.; Reiher, M.; Roos, B. O.; Serrano-Andrés, L.; Urban, M.; Veryazov, V.; Lindh, R. MOLCAS 7: The Next Generation. *J. Comput. Chem.* **2010**, *31* (1), 224−247.
(37) Veryazov, V.; Widmark, P.-O.; Serrano-Andrés, L.; Lindh, R.; Roos, B. O. 2MOLCAS as a development platform for quantum chemistry software. *Int. J. Quantum Chem.* **2004**, *100* (4), 626−635.
(38) Karlstrom, G.; Lindh, R.; Malmqvist, P. A.; Roos, B. O.; Ryde, U.; Veryazov, V.; Widmark, P. O.; Cossi, M.; Schimmelpfennig, B.; Neogrady, P.; Seijo, L. MOLCAS: a program package for computational chemistry. *Comput. Mater. Sci.* **2003**, *28* (2), 222−239.
(39) Habib, F.; Luca, O. R.; Vieru, V.; Shiddiq, M.; Korobkov, I.; Gorelsky, S. I.; Takase, M. K.; Chibotaru, L. F.; Hill, S.; Crabtree, R. H.; Murugesu, M. Influence of the Ligand Field on Slow Magnetization Relaxation versus Spin Crossover in Mononuclear Cobalt Complexes. *Angew. Chem., Int. Ed.* **2013**, *52* (43), 11290−11293.
(40) Langley, S. K.; Ungur, L.; Chilton, N. F.; Moubaraki, B.; Chibotaru, L. F.; Murray, K. S. Single-Molecule Magnetism in a Family of {CoIII2DyIII2} Butterfly Complexes: Effects of Ligand Replacement on the Dynamics of Magnetic Relaxation. *Inorg. Chem.* **2014**, *53* (9), 4303−4315.
(41) Roos, B. O.; Lindh, R.; Malmqvist, P.-Å.; Veryazov, V.; Widmark, P.-O.; Borin, A. C. New Relativistic Atomic Natural Orbital Basis Sets for Lanthanide Atoms with Applications to the Ce Diatom and LuF3. *J. Phys. Chem. A* **2008**, *112* (45), 11431−11435.
(42) Ungur, L.; Thewissen, M.; Costes, J.-P.; Wernsdorfer, W.; Chibotaru, L. F. Interplay of Strongly Anisotropic Metal Ions in Magnetic Blocking of Complexes. *Inorg. Chem.* **2013**, *52* (11), 6328−6337.
(43) Angel, R. J.; Alvaro, M.; Gonzalez-Platas, J. EosFit7c and a Fortran module (library) for equation of state calculations. *Z. Kristallogr. - Cryst. Mater.* **2014**, *229* (5), 405.
(44) Gonzalez-Platas, J.; Alvaro, M.; Nestola, F.; Angel, R. EosFit7-GUI: a new graphical user interface for equation of state calculations, analyses and teaching. *J. Appl. Crystallogr.* **2016**, *49* (4), 1377−1382.
(45) Angel, R. J.; Alvaro, M.; Miletich, R.; Nestola, F. A simple and generalised P−T−V EoS for continuous phase transitions, implemented in EosFit and applied to quartz. *Contrib. Mineral. Petrol.* **2017**, *172* (5), 29.
(46) Casanova, D.; Alemany, P.; Bofill, J. M.; Alvarez, S. Shape and Symmetry of Heptacoordinate Transition-Metal Complexes: Structural Trends. *Chem. - Eur. J.* **2003**, *9* (6), 1281−1295.
(47) Campbell, V. E.; Guillot, R.; Riviere, E.; Brun, P.-T.; Wernsdorfer, W.; Mallah, T. Subcomponent Self-Assembly of Rare-Earth Single-Molecule Magnets. *Inorg. Chem.* **2013**, *52* (9), 5194−5200.
(48) Gagliardi, L.; Lindh, R.; Karlström, G. Local properties of quantum chemical systems: The LoProp approach. *J. Chem. Phys.* **2004**, *121* (10), 4494−4500.
(49) Aravena, D.; Ruiz, E. Shedding Light on the Single-Molecule Magnet Behavior of Mononuclear DyIII Complexes. *Inorg. Chem.* **2013**, *52* (23), 13770−13778.
(50) Chibotaru, L. F.; Ungur, L.; Soncini, A. The Origin of Nonmagnetic Kramers Doublets in the Ground State of Dysprosium Triangles: Evidence for a Toroidal Magnetic Moment. *Angew. Chem., Int. Ed.* **2008**, *47* (22), 4126−4129.
(51) Briganti, M.; Garcia, G. F.; Jung, J.; Sessoli, R.; Le Guennic, B.; Totti, F. Covalency and magnetic anisotropy in lanthanide single molecule magnets: the DyDOTA archetype. *Chem. Sci.* **2019**, *10* (30), 7233−7245.
(52) Singh, S. K.; Gupta, T.; Ungur, L.; Rajaraman, G. Magnetic Relaxation in Single-Electron Single-Ion Cerium(III) Magnets: Insights from Ab Initio Calculations. *Chem. - Eur. J.* **2015**, *21* (39), 13812−13819.
(53) Ou-Yang, J. K.; Saleh, N.; Fernandez Garcia, G.; Norel, L.; Pointillart, F.; Guizouarn, T.; Cador, O.; Totti, F.; Ouahab, L.;

DOI: 10.1021/acs.inorgchem.9b02962
Inorg. Chem. 2020, 59, 717−729

Crassous, J.; Le Guennic, B. Improved slow magnetic relaxation in optically pure helicene-based DyIII single molecule magnets. *Chem. Commun.* **2016**, *52* (100), 14474−14477.
(54) Holmberg, R. J.; Ho, L. T. A.; Ungur, L.; Korobkov, I.; Chibotaru, L. F.; Murugesu, M. Observation of unusual slow-relaxation of the magnetisation in a Gd-EDTA chelate. *Dalton Transactions* **2015**, *44* (47), 20321−20325.
(55) Guo, Y.-N.; Xu, G.-F.; Wernsdorfer, W.; Ungur, L.; Guo, Y.; Tang, J.; Zhang, H.-J.; Chibotaru, L. F.; Powell, A. K. Strong Axiality and Ising Exchange Interaction Suppress Zero-Field Tunneling of Magnetization of an Asymmetric Dy2 Single-Molecule Magnet. *J. Am. Chem. Soc.* **2011**, *133* (31), 11948−11951.

DOI: 10.1021/acs.inorgchem.9b02962
Inorg. Chem. 2020, 59, 717−729